Bulk magnetic domain stability controls paleointensity fidelity

Greig A. Paterson[a,b,1], Adrian R. Muxworthy[c], Yuhji Yamamoto[d], and Yongxin Pan[a,b,e]

[a]Key Laboratory of Earth and Planetary Physics, Institute of Geology and Geophysics, Chinese Academy of Sciences, Beijing 100029, China; [b]Institutions of Earth Science, Chinese Academy of Sciences, Beijing 100029, China; [c]Department of Earth Science and Engineering, Imperial College London, London SW7 2AZ, United Kingdom; [d]Center for Advanced Marine Core Research, Kochi University, Nankoku 783-8502, Japan; and [e]College of Earth Sciences, University of Chinese Academy of Sciences, Beijing 100049, China

Edited by Lisa Tauxe, University of California, San Diego, La Jolla, CA, and approved November 2, 2017 (received for review August 8, 2017)

Nonideal, nonsingle-domain magnetic grains are ubiquitous in rocks; however, they can have a detrimental impact on the fidelity of paleomagnetic records—in particular the determination of ancient magnetic field strength (paleointensity), a key means of understanding the evolution of the earliest geodynamo and the formation of the solar system. As a consequence, great effort has been expended to link rock magnetic behavior to paleointensity results, but with little quantitative success. Using the most comprehensive rock magnetic and paleointensity data compilations, we quantify a stability trend in hysteresis data that characterizes the bulk domain stability (BDS) of the magnetic carriers in a paleomagnetic specimen. This trend is evident in both geological and archeological materials that are typically used to obtain paleointensity data and is therefore pervasive throughout most paleomagnetic studies. Comparing this trend to paleointensity data from both laboratory and historical experiments reveals a quantitative relationship between BDS and paleointensity behavior. Specimens that have lower BDS values display higher curvature on the paleointensity analysis plot, which leads to more inaccurate results. In-field quantification of BDS therefore reflects low-field bulk remanence stability. Rapid hysteresis measurements can be used to provide a powerful quantitative method for preselecting paleointensity specimens and postanalyzing previous studies, further improving our ability to select high-fidelity recordings of ancient magnetic fields. BDS analyses will enhance our ability to understand the evolution of the geodynamo and can help in understanding many fundamental Earth and planetary science questions that remain shrouded in controversy.

paleomagnetism | paleointensity | rock magnetism | magnetic domain state

The strength of the ancient geomagnetic field (paleointensity) is an invaluable tool for understanding the evolution of the geodynamo and how it interacts with other Earth systems, as well as understanding our solar system. As such, paleointensity data have important applications in understanding the early geodynamo (1, 2) and mantle convection (3), they can be used as a dating tool (4), they have been used to suggest links between the geomagnetic field and climate (5), and paleointensity data can provide important constraints on the evolution of the early solar system (6). However, the interpretation of paleointensity data, and hence their applications, remains controversial due to the difficulty in the acquisition and identification of reliable data. Developing robust methods to enhance paleointensity data fidelity is, therefore, one of the most enduring challenges of solid Earth geophysical studies.

Although progress has been made in this endeavor (7–12), no developed approach represents a direct measure of properties that govern the acquisition of thermoremanent magnetization (TRM). Linking paleointensity results to the fundamental rock magnetic properties that should inform us of the stability of paleomagnetic recordings has been a long-sought-after but unfulfilled goal (13–18). While a qualitative link between magnetic particle grain size (hence magnetic domain state) and paleointensity behavior is established (19, 20) and quantitative measures for such synthetic specimens exist (21), these measures are not unambiguous proxies of fundamental magnetic properties and may be influenced by other detrimental factors (22–24). Quantitative links between direct measures of fundamental rock magnetic properties that can be applied to natural specimens and the fidelity of paleointensity results are lacking.

Magnetic hysteresis measurements of coercivity (B_c), saturation (M_s), and remanent (M_{rs}) magnetizations, combined with back-field saturation remanence demagnetization measurements of remanent coercivity (B_{cr}), are the most widely used and rapid rock magnetic measurements in paleomagnetic studies (e.g., the 112 studies presented in Datasets S1–S3). As such, these have been extensively investigated as potential tools for preselecting paleointensity specimens for success and postanalyzing paleointensity data (15–18). A well-established method of presenting this type of hysteresis data is to compare M_{rs}/M_s to B_{cr}/B_c (25). Although frequently misinterpreted as being a definitive indicator of magnetic grain size, this style of plot is also sensitive to grain size distributions, magnetic interactions, mineralogy, and thermal fluctuations, among other factors (26–29). Because of this, an M_{rs}/M_s versus B_{cr}/B_c plot is only indicative of the relative magnetic stability of a collection of specimens.

Here, we use B_{cr}/B_c and M_{rs}/M_s data from sized (titano-) magnetite specimens to develop a measure of the relative bulk domain stability (BDS) of a paleomagnetic specimen. Then, using hysteresis and paleointensity data from new laboratory control data and a compilation of historical data, we demonstrate that a

Significance

The strength of the ancient geomagnetic field (paleointensity) is a key tool to observe the evolution of early Earth's geodynamo, which provided an essential protective barrier for the emergence of life. However, paleointensity data are fraught with difficulties that make understanding the evolution of our planet more challenging. We demonstrate a long-sought-after quantitative relationship between fundamental rock magnetic properties and the fidelity of paleointensity records. This relationship can be used to reject low-fidelity paleointensity records and help resolve controversy that surrounds key questions about the evolution of our planet, such as when did the geodynamo begin, when did the inner core solidify, or how early life may have interacted with the magnetic field.

Author contributions: G.A.P. designed research; G.A.P. performed research; G.A.P., A.R.M., and Y.Y. analyzed data; and G.A.P., A.R.M., Y.Y., and Y.P. wrote the paper.

The authors declare no conflict of interest.

This article is a PNAS Direct Submission.

Data deposition: All data are available from the MagIC database (https://www2.earthref.org/MagIC).

[1]To whom correspondence should be addressed. Email: greig.paterson@mail.iggcas.ac.cn.

This article contains supporting information online at www.pnas.org/lookup/suppl/doi:10.1073/pnas.1714047114/-/DCSupplemental.

quantifiable relationship exists between the BDS of a paleomagnetic specimen and the behavior and accuracy of Thellier-type paleointensity results. This relationship, which may be widespread throughout all paleomagnetic studies, represents an important means of understanding the fundamental controls on paleointensity data and identifying high-fidelity results.

Results

One of the challenges in identifying links between paleointensity data and fundamental rock magnetic properties is that datasets are often small and can be diverse, which means that relationships in one dataset are often not observed in another (cf. refs. 15 and 17). To overcome this, we use a compilation of 303 hysteresis data from a diverse set of sized (titano-) magnetite specimens to define a base trend with which all datasets can be referenced (referred to as the "Sized Dataset"; Dataset S1).

When viewed in $\log_{10}$ space, these hysteresis data form a linear trend that can be decomposed with principal component analysis (PCA). This first principal component accounts for 98.3% of the dataset variance (red line in Fig. 1*A*). The position of hysteresis data projected on this axis can be viewed as a relative measure of "effective BDS" (i.e., an approximate quantitative measure of the effective bulk domain state of an assemblage of magnetic carriers that may be influenced by one or more factor; see *Methods* for calculation details). This is evidenced by a strong correlation between BDS and the known grain size of these specimens (Fig. 1*B*), as well as strong relations with single-domain (SD) and multidomain (MD) mixing trends (26), and increasing degrees of magnetostatic interactions (27) (Fig. S1). BDS is a relative measure of stability where larger values are indicative of more stable remanence carriers (e.g., an idealized assemblage of Stoner–Wohlfarth particles has a BDS of 0.79) and smaller, more negative values indicate less stable remanence carriers (e.g., a 220-μm grain has a BDS of −0.94; Fig. 1*B* and Dataset S1).

By defining the BDS trend using the Sized Dataset, any hysteresis data can be projected onto the same BDS trend, irrespective of the material or the number of data available. BDS accounts for 96.3% and 94.0% of the data variances from 2,682 geological specimens ("Geological Dataset") and 504 archeological specimens ("Archeological Dataset"), respectively—materials that are typically used to obtain paleointensity data (Fig. 1 *C* and *D* and Datasets S2 and S3). This BDS trend is therefore dominant throughout paleomagnetic and archeomagnetic datasets, and, irrespective of the underlying mechanisms, BDS represents a relative measure of the magnetic domain stability of a bulk paleomagnetic specimen.

Using hysteresis and paleointensity data from new control data, historical data, and both datasets combined ("Control," "Historical," and "Combined" Datasets, respectively), we find clear relationships between BDS and the inaccuracy of the paleointensity results (Fig. 2 *A*, *D*, and *G*). No consistent relationship is found with respect to inaccuracy and hysteresis ratios B_{cr}/B_c and M_{rs}/M_s (Table S2). We only consider correlations robust if they are present in the Control, Historical, and Combined Datasets. This suggests that BDS is more robust to the diversity of materials, experimental steps, different laboratory field conditions, and sample heterogeneity (the historical hysteresis data were measured on sister specimens to the paleointensity data). For the Control Dataset, in which all experimental conditions are near-identical, the relation between inaccuracy and BDS is more clearly defined than for the Historical

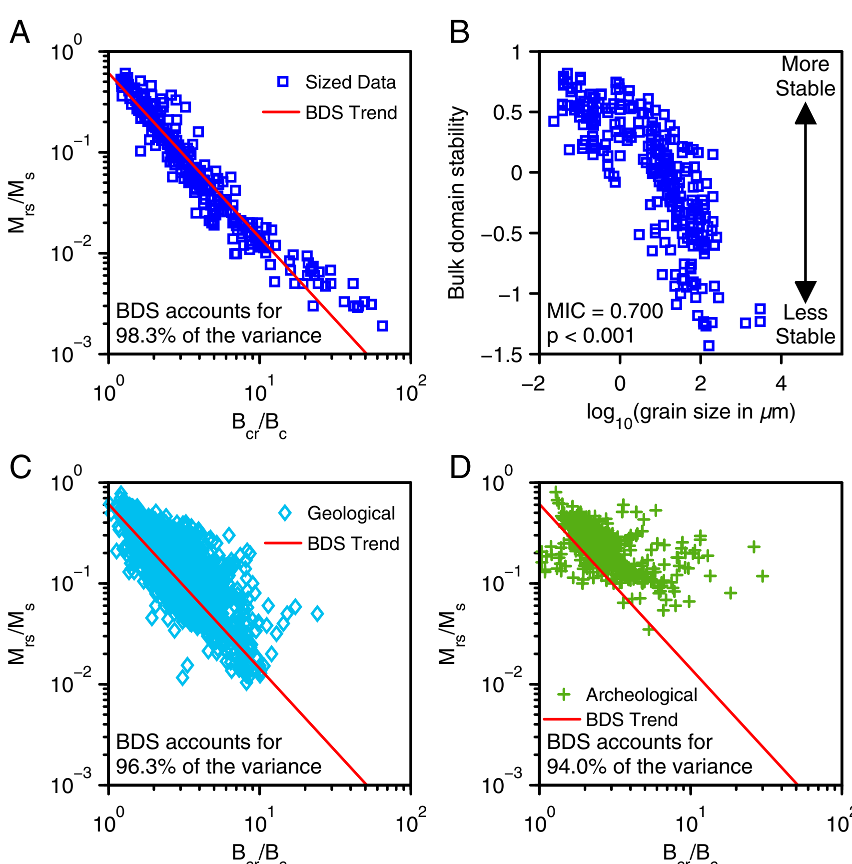

Fig. 1. PCA of hysteresis data. (*A*) The 303 sized magnetite data that define the BDS trend. (*B*) The relation between BDS and the physical magnetic grain size ($n = 303$). Hysteresis data from (*C*) 2,682 geological and (*D*) 504 archeological specimens typically used for paleointensity studies. The BDS trend is prevalent throughout all datasets.

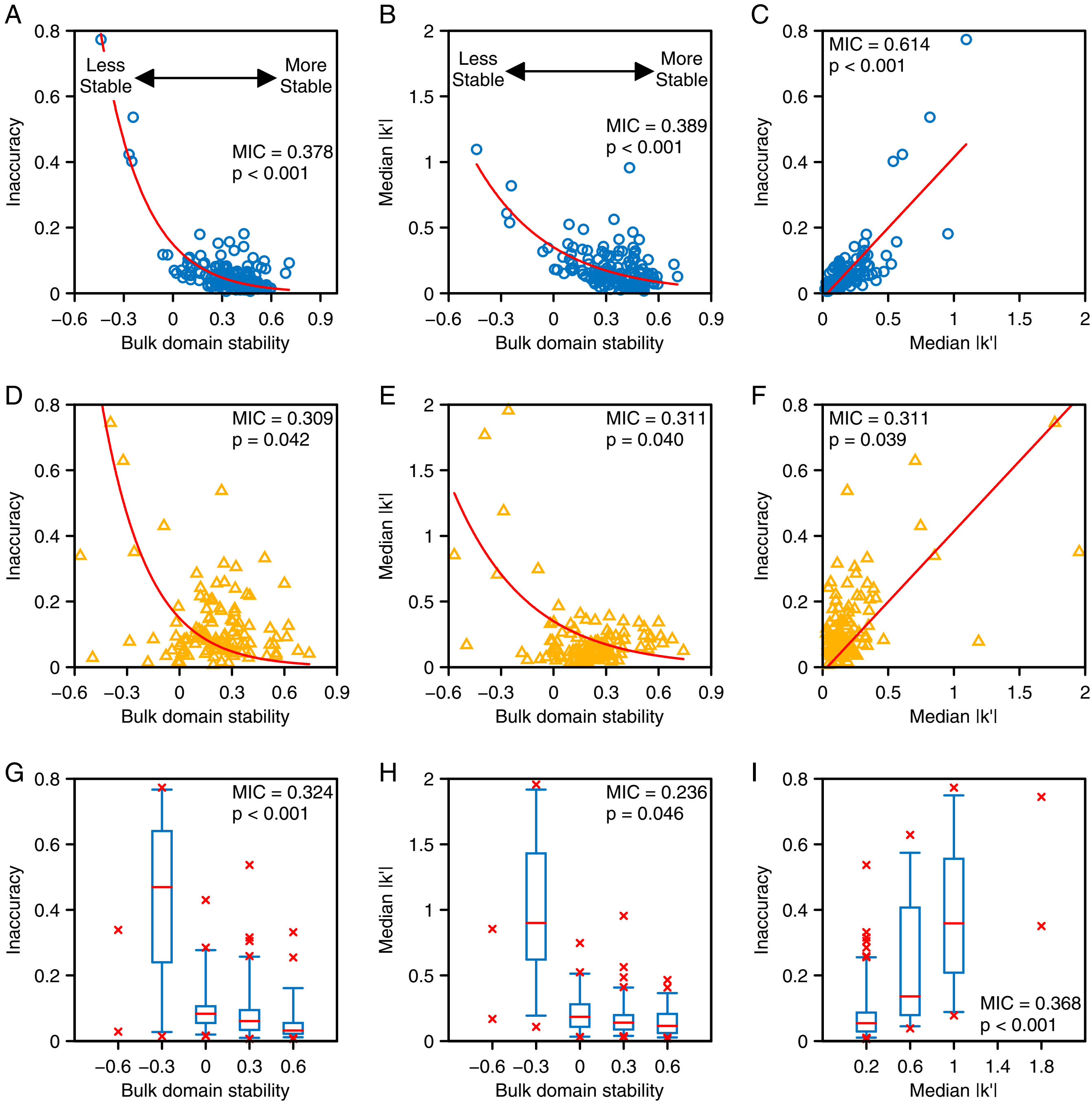

Fig. 2. Comparison between BDS and the inaccuracy and curvature of paleointensity data. Comparison of median inaccuracy and median Arai plot curvature with bulk domain stability, and the median inaccuracy as a function of Arai plot curvature, $|k'|$, for (*A*–*C*) the 160 Control data, (*D*–*F*) the 112 Historical data, and (*G*–*I*) both datasets combined ($n = 272$). An ideal paleointensity result has a linear Arai plot, which corresponds to a curvature of zero. MIC is the maximal information coefficient of ref. 47 and is a measure of the strength of the relationship between two variables. In parts *A*–*F*, the red lines represent best-fit models to the Control Dataset where an exponential function was used for *A* and *B*, and a linear function was used in *C*. In *G* and *H*, the boxes denote the IQRs, the whiskers denote the 95% ranges, and the red lines are the median values. The red crosses represent values that lie outside the 95% ranges. Box and whiskers are only shown if ≥5 data are available; otherwise, cross symbols are used.

Dataset (Fig. 2). Nevertheless, both indicate that paleointensity accuracy deteriorates as BDS decreases (Fig. 2 *A*, *D*, and *G*).

Median curvature of the fitted analysis, or Arai plot segments (21, 30), increases with decreasing BDS for all datasets (Fig. 2 *B*, *E*, and *H*). That is, less magnetically stable specimens tend to produce more nonlinear Arai plots (an ideal result is a straight line), which confirms that the trend isolated from high-field hysteresis data corresponds to a low-field bulk remanence stability trend. The inaccuracy of these datasets is strongly correlated with Arai curvature, $|k'|$, indicating that nonlinearity is the source of incorrect results and that inaccuracy, curvature, and BDS are intimately related (Fig. 2 *C*, *F*, and *I*). These findings illustrate that, when interpreted appropriately, an M_{rs}/M_s versus B_{cr}/B_c plot is still a valuable rock magnetic tool.

For statistics typically used to quantify partial TRM (pTRM) checks and tails (statistics thought to be sensitive to domain state-related remanence instability), none are consistently correlated with B_{cr}/B_c or M_{rs}/M_s for all datasets (Table S2). However, both Arai plot curvature and pTRM check "DRAT" are consistently sensitive to BDS. Of all statistics typically used to quantify pTRM checks and tails, only Arai plot curvature is consistently related to the inaccuracy of the paleointensity results (Fig. 2 *C*, *F*, and *I* and Table S3). Arai plot curvature is therefore one of the most useful selection criteria for distinguishing unstable remanence carriers and the inaccurate results they produce.

Discussion

Summary. We have quantified a trend in hysteresis data that corresponds to the BDS of a paleomagnetic specimen, irrespective of the specific mechanisms that are influencing the specimen's bulk domain state (i.e., grain size, size distributions, magnetic interactions, etc.). BDS is correlated to the curvature and accuracy of paleointensity results, and therefore also represents a measure of bulk remanence stability. Such relations have long been hypothesized, but have not been conclusively identified for natural materials used for paleointensity studies.

Previous efforts to identify rock magnetic properties related to paleointensity have been applied to relatively small numbers of specimens (31), applied to ancient materials where the true field strength is unknown (15), associated paleointensity and hysteresis data at the site and not sample level, or only considered a single acceptable result per specimen out of many possible acceptable results (15, 17). These factors can make it difficult to identify general trends in complicated datasets (examples of these effects are outlined in *SI Factors That Can Obscure BDS Relationships*). Our analysis of 272 paleointensity data, application of minimal data selection, and intimately associated paleointensity and hysteresis data, along with consideration of all possible paleointensity results for each specimen, avoids these issues, allowing us to highlight underlying trends.

Robustness of Relationships. The laboratory Control Dataset is well characterized with consistent paleointensity experiment conditions and clearly illustrates the relationships identified here (e.g., Fig. 2 *A*–*C*). The Historical Dataset, on the other hand, is more complicated. The specimens are fresh (not thermally stabilized) and therefore more likely to chemically alter during experimental heating, they were measured in different laboratories with different experimental steps and applied field strengths and angles, the ratios of the laboratory to ancient field strengths were different, and, furthermore, hysteresis data were measured on sister specimens; hence sample heterogeneity may be important. Despite these complications, we can still identify significant trends in Arai plot curvature and paleointensity inaccuracy that are related to the specimens' BDS (Fig. 2 *D*–*F*). The "dirtiness" of the Historical Dataset therefore emphasizes the robustness of these relations.

Alternative Quantifications of BDS. Our analysis characterizes a relative measure of BDS, but cannot reveal the mechanisms that underlie the variability in stability that influences paleointensity results. A number of alternative data measurements and/or analyses may provide more powerful discrimination as to the specific underlying mechanisms leading to low BDS values and poor paleointensity results. The recent rapid advancement of first-order reversal curve analysis looks to be the most promising tool to achieve this (15, 32–34). A future challenge is therefore to develop suitably large datasets to test and develop these ideas.

Other Paleointensity Methods. All Control and Historical paleointensity data presented here come from the Coe variant of Thellier-type experiments (35), and, although paleointensity results from different Thellier-type methods can have distinct behavior with respect to differing domain state (30), BDS should manifest in some fashion in all paleointensity data. This may not only be related to Arai plot curvature, but may, for example, manifest in Arai plot zigzagging for "IZZI"-protocol experiments (36). At present, however, insufficient data are publically available to explore this in more detail.

Sufficient data are available from nonheating pseudo-Thellier experiments to illustrate the influence of BDS on this paleointensity method (37). We show that the calibration factor used to scale an anhysteretic remanent magnetization (ARM) is dependent on BDS such that lower BDS values yield lower calibration factors (Fig. 3*A*). This relationship could be used for screening out less stable specimens for use in pseudo-Thellier experiments, or, with a larger and more diverse dataset, BDS could be used to determine specimen specific pseudo-Thellier calibrations factors.

Geological materials form the bulk of our analyses, but the BDS trend is also evident in archeological materials (Fig. 1*D*). A more widespread application of hysteresis to archeological materials would make BDS a valuable tool in archeomagnetic studies.

Impact on Other Paleomagnetic Studies. The prevalence of the BDS trend in paleomagnetic specimens (Fig. 1) suggests this behavior should impact all paleomagnetic studies on volcanic materials, not just paleointensity data. For the Control Dataset, we find the median destructive field (MDF) of ARM and TRM are both correlated with BDS (Fig. 3 *B* and *C*). For the Historical Dataset, where the natural remanent magnetizations should be TRMs, a similar relation is observed (Fig. 3*C*). Specimens with low BDS will be more susceptible to overprinting and remagnetization, which may influence the interpretation of directional data used for secular variation, magnetostratigraphy, or tectonic reconstructions. This type of information, which is invaluable for asserting directional fidelity, may not be possible to directly extract from the demagnetization data, but the hysteresis analysis outlined in this work would be an alternative approach to assert reliability.

Applications of BDS. BDS determined from hysteresis data has the potential to be used as a statistic to preselect specimens for paleointensity experiments or to reject results during analysis. Although many such statistics exist (12), all are derived from paleointensity data, and none represent a direct measure of magnetic properties that govern the acquisition of TRM. BDS, however, does reflect fundamental magnetic properties. Deviations from the trends identified here (e.g., specimens with high BDS, but high Arai plot curvature) also provide an approach for identifying specimens strongly influenced by other detrimental factors, such as alteration or chemical magnetizations.

Combining both the Control and Historical Datasets, we explore how different thresholds for BDS influence the median inaccuracy and its interquartile range (IQR) when specimens with low stability are rejected (Fig. 3*D*). For this dataset, there is a change in slope in both the median inaccuracy and IQR at BDS values of ∼0.10, which yield more accurate and less scattered results (Fig. 3*D*). This corresponds to B_{cr}/B_c and M_{rs}/M_s ratios of ∼3.4 and ∼0.08, respectively. Specimens that are less stable than a BDS of 0.10 are less likely to yield meaningful paleointensity estimates. This first-order threshold can be used as a preselection criterion in combination with other data selection processes. From the compilation of 2,682 geological specimens, ∼18% have BDS values < 0.10, which suggests that less than 20% of paleomagnetic specimens have such low bulk domain stabilities that they can be viewed as poor paleomagnetic carriers that are less likely to yield geophysically meaningful results.

The search to identify reliable paleointensity data is as old as the discipline itself, but, despite this longevity, all current approaches do not directly quantify the fundamental magnetic properties that govern the acquisition of TRM. We have demonstrated that, by quantifying hysteresis data in terms of the BDS of the entire magnetic assemblage in a paleomagnetic specimen, we can relate rock magnetic properties to the behavior and reliability of paleointensity data. This powerful tool will strengthen our ability to probe the workings of our planet's deep interior in greater detail and with greater confidence.

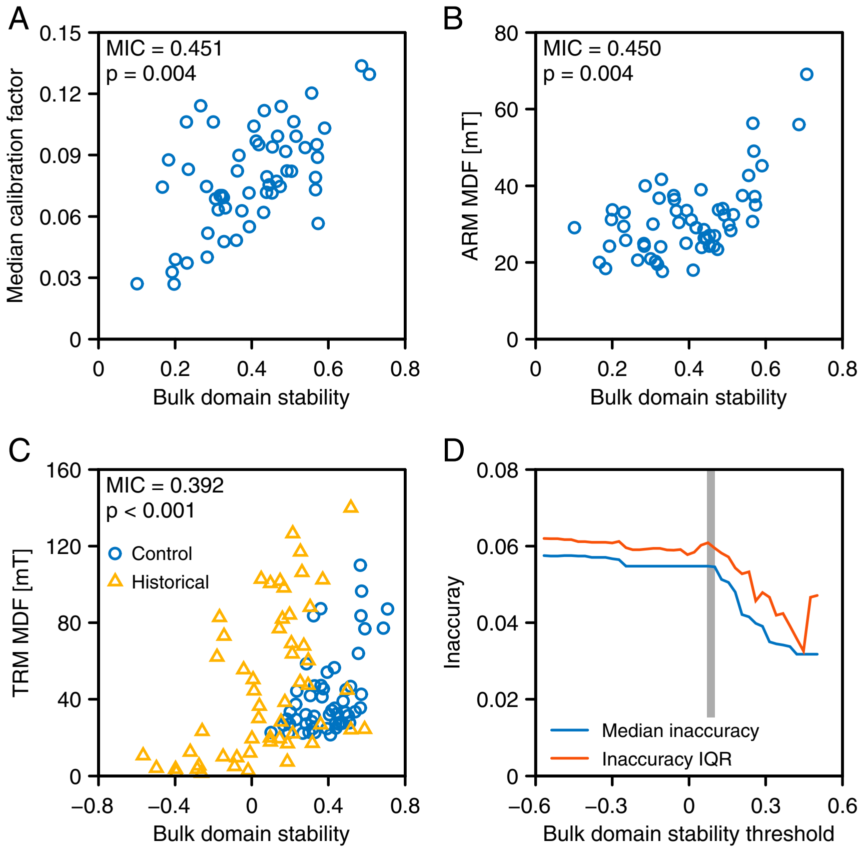

Fig. 3. Relationships between BDS and other paleomagnetic results and how BDS can be used to improve paleointensity results. BDS relationship with (*A*) calibration of the pseudo-Thellier method (n = 56), (*B*) ARM MDF from 56 Control data, and (*C*) TRM MDF from 56 Control and 55 Historical data. In *C*, MIC values are for the Control and Historical Datasets combined. (*D*) Median inaccuracy and IQR after rejecting specimens with BDS less than the given thresholds. The selection thresholds are applied to the Control and Historical Datasets combined. The gray shaded area represents a change in the slopes that yields more accurate and less scattered results and may be a useful first-order selection threshold for preselecting paleointensity specimens.

Methods

Hysteresis Data. For the sized magnetite data presented in Fig. 1 *A* and *B*, 303 hysteresis ratio combinations (i.e., B_{cr}/B_c and M_{rs}/M_s) were compiled from the published literature. These titanomagnetite and magnetite specimens come from 34 studies and represent a wide range of synthesis methods, grain sizes (and grain size distribution), and grain spacing (magnetic interactions), as well as differing degrees of annealing. So, although dominated by grain size effects, the hysteresis data are influenced by a wide range of other factors. The data and sources are given in Dataset S1. Similarly, 2,682 hysteresis data from geological materials and 504 archeological data were compiled from the literature and are detailed in Datasets S2 and S3, respectively.

For the Control Dataset, some hysteresis and backfield measurements were previously measured (37). New data were measured using a Princeton Measurements Corporation MicroMag 3900 Vibrating Sample Magnetometer at the Institute of Geology & Geophysics, Chinese Academy of Sciences (IGGCAS). For the Historical Dataset, previously published hysteresis data were used, and we refer to the relevant studies (8, 17, 37–41). All hysteresis measurements were reprocessed following ref. 42, except for 11 sized magnetite specimens included in the Control Dataset (8, 41), where the reported hysteresis ratios were used. Where multiple hysteresis data were available per paleointensity specimen, hysteresis data were averaged. Only hysteresis data that have acceptable paleointensity results are analyzed for the Control and Historical Datasets. Additional descriptions of the all of the datasets are given in *SI Dataset Descriptions*, Figs. S2 and S3, and Table S1.

BDS. To identify the BDS trend, the Sized Dataset hysteresis data are $\log_{10}$-transformed and detrended by the mean values, before performing PCA. BDS values are calculated by projecting the hysteresis data onto the first principal component (an illustrative example is given in Fig. S5). We normalize BDS such that a single grain yielding a perfectly square hysteron has a BDS value of 1. If X represents B_{cr}/B_c data and Y represents M_{rs}/M_s data, BDS values are given by

$$BDS = -0.3900[\log_{10}(X) - 0.6062] + 0.6353[\log_{10}(Y) + 1.2018]. \quad [1]$$

Since the hysteresis ratios are detrended for the dataset means, the origin of the BDS axis corresponds to center of mass of the Sized Dataset; BDS is therefore only a relative scale. An idealized Stoner–Wohlfarth assemblage (B_{cr}/B_c = 1.09, M_{rs}/M_s = 0.5) (43, 44) has a BDS of 0.79, while an assemblage of idealized cubic anisotropy dominated particles (B_{cr}/B_c = 1.08, M_{rs}/M_s = 0.87) (45) has a BDS of 0.95. The lowest value is $-\infty$ and represents a specimen incapable of retaining any magnetic remanence over measurement timescales (i.e., superparamagnetic grains). The full principal component description is given in *SI Methods*.

Paleointensity Experiments. Only the Control and Historical Dataset are associated with paleointensity data. All paleointensity data are from the Coe paleointensity protocol (35), whereby a specimen's original magnetization is progressively removed and replaced by a laboratory-induced magnetization by heating the specimen to increasingly higher temperatures.

New "control" paleointensity experiments were performed using 62 specimens from refs. 17 and 39, 10 from ref. 46, and 79 new basalts, dikes, granites, and granitoids (see *SI Dataset Descriptions*). All specimens were thermally stabilized before the experiments, to ensure no alteration occurred, and given a full laboratory TRM from 700 °C. Magnetite (with some titanomagnetite) and hematite are the main magnetic carriers in these specimens (37). The paleointensity experiments involved 7 to 12 heating steps up to a peak temperature of 700 °C and included pTRM and tail checks. All remanences were acquired in a field of 32 μT applied along the same axis. Remanence measurements were performed at IGGCAS with a 2G Enterprises superconducting magnetometer. Within the Control Dataset, we also include 11 Coe protocol paleointensity data from previously measured sized magnetite specimens available from the MagIC database (8, 41). With the exception of the sized magnetite specimens, all Control Dataset paleointensities were measured on the same specimen as for the hysteresis measurements following thermal stabilization.

Historical paleointensity data are available from the MagIC database. From a total of 172 Coe protocol paleointensity data, 129 are associated with hysteresis data at the core or clast level (17, 38, 40); hysteresis and paleointensity data were measured on sister specimens. Titanomagnetite with and without hematite are the main magnetic carriers in these specimens (17, 38, 40).

Paleointensity Analysis. To quantify a specimen's general behavior, instead of considering only a single Arai plot fit per specimen, we consider all fits. We also apply a minimal set of selection criteria to ensure robust basic fitting: We require that at least four Arai plot points per fit ($n \geq 4$), "FRAC" $\geq$ 0.45, and unanchored "MAD" ≤ 15°. We apply no other criteria to avoid distortion of any relationship with BDS.

For the Historical Dataset, in addition to the above criteria, to minimize the potential impact of magnetomineralogical alteration, each fit is required to have pTRM checks "δpal" ≤ 20 and "δCK" ≤ 10. These thresholds correspond to the 95th percentiles of the accepted fits from the Control Dataset and should therefore be predominantly screening out the effects of alteration.

All paleointensity statistics are calculated following the standard definitions (12) and are calculated as median values of the accepted results. To obtain a reasonable measure of a specimen's general behavior, we require at least three Arai plot fits per specimen. After applying these requirements, two Control and 17 Historical specimens are rejected.

The inaccuracy of a paleointensity result (B_{Anc}) is based on the deviation (*Dev.*) from the correct intensity (B_{Exp}): $Dev. = \ln(B_{Anc}/B_{Exp})$, where negative values are underestimates of the true intensity, and positive values are overestimates (21). Inaccuracy is quantified as the median absolute deviation of all acceptable fits, such that values of 0 are perfectly correct.

Pseudo-Thellier data are taken from ref. 37 and are their unselected results. These are the median calibration factors from all possible fits on the pseudo-Arai plots with at least four data points (37).

MDF Analysis. Control Dataset results were taken from ref. 37, and Historical results were taken from ref. 17. All remanences are approximately univectoral, so no additional adjustments were made to calculate the MDFs.

Correlations. All correlations are performed using the maximal information coefficient (MIC) (47), which varies between 0 and 1. The MIC places no constraint on the form of the relationship, which makes it a flexible method for assessing diverse types of relationships. The default grid scaling parameter $\alpha = 0.6$ was used (47). *P* values are calculated by interpolating the reference tables and are conservatively reported as *p* plus its associated 95% confidence interval and are considered significant if ≤ 0.05.

ACKNOWLEDGMENTS. We thank Jinpeng Sun and Yongjie Hou for assistance with some measurements. We are grateful to Mimi Hill, Catherine Kissel, Ron Shaar, Aleksey Smirnov, Yoichi Usui, and Huiru Xu for providing data used in Fig. 1. We also thank Josh Feinberg and an anonymous reviewer for their helpful comments. G.A.P. acknowledges funding from National Natural Science Foundation China (NSFC) Grants 41374072 and 41574063. Y.P. and G.A.P. acknowledge NSFC Grant 41621004 and CAS Project XDB18010203.

1. Tarduno JA, Cottrell RD, Davis WJ, Nimmo F, Bono RK (2015) A Hadean to Paleoarchean geodynamo recorded by single zircon crystals. *Science* 349:521–524.
2. Biggin AJ, et al. (2015) Palaeomagnetic field intensity variations suggest Mesoproterozoic inner-core nucleation. *Nature* 526:245–248.
3. Biggin AJ, et al. (2012) Possible links between long-term geomagnetic variations and whole-mantle convection processes. *Nat Geosci* 5:526–533.
4. Aitken MJ (1990) *Science-Based Dating in Archaeology* (Longman, London).
5. Knudsen MF, Riisager P (2009) Is there a link between Earth's magnetic field and low-latitude precipitation? *Geology* 37:71–74.
6. Wang H, et al. (2017) Lifetime of the solar nebula constrained by meteorite paleomagnetism. *Science* 355:623–627.
7. Selkin PA, Tauxe L (2000) Long-term variations in palaeointensity. *Phil Trans R Soc Lond A* 358:1065–1088.
8. Krása D, Heunemann C, Leonhardt R, Petersen N (2003) Experimental procedure to detect multidomain remanence during Thellier-Thellier experiments. *Phys Chem Earth* 28:681–687.
9. Leonhardt R, Heunemann C, Krása D (2004) Analyzing absolute paleointensity determinations: Acceptance criteria and the software ThellierTool4.0. *Geochem Geophys Geosyst* 5:Q12016.
10. Chauvin A, Roperch P, Levi S (2005) Reliability of geomagnetic paleointensity data: The effects of the NRM fraction and concave-up behavior on paleointensity determinations by the Thellier method. *Phys Earth Planet Inter* 150:265–286.
11. Biggin AJ, Paterson GA (2014) A new set of qualitative reliability criteria to aid inferences on palaeomagnetic dipole moment variations through geological time. *Front Earth Sci* 2:24.
12. Paterson GA, Tauxe L, Biggin AJ, Shaar R, Jonestrask LC (2014) On improving the selection of Thellier-type paleointensity data. *Geochem Geophys Geosyst* 15: 1180–1192.
13. Haag M, Dunn JR, Fuller MD (1995) A new quality check for absolute palaeointensities of the Earth magnetic field. *Geophys Res Lett* 22:3549–3552.
14. Cui YL, Verosub KL, Roberts AP, Kovacheva M (1997) Mineral magnetic studies of archaeological samples: Implications for sample selection for paleointensity determinations. *J Geomag Geoelectr* 49:567–585.
15. Carvallo C, et al. (2006) Increasing the efficiency of paleointensity analyses by selection of samples using first-order reversal curve diagrams. *J Geophys Res* 111:B12103.
16. Michalk DM, Muxworthy AR, Böhnel HN, Maclennan J, Nowaczyk NR (2008) Evaluation of the multispecimen parallel differential pTRM method: A test on historical lavas from Iceland and Mexico. *Geophys J Int* 173:409–420.
17. Paterson GA, Muxworthy AR, Roberts AP, Mac Niocaill C (2010) Assessment of the usefulness of lithic clasts from pyroclastic deposits for paleointensity determination. *J Geophys Res* 115:B03104.
18. Calvo-Rathert M, Morales-Contreras J, Carrancho Á, Goguitchaichvili A (2016) A comparison of Thellier-type and multispecimen paleointensity determinations on Pleistocene and historical lava flows from Lanzarote (Canary Islands, Spain). *Geochem Geophys Geosyst* 17:3638–3654.
19. Levi S (1977) Effect of magnetite particle size on paleointensity determinations of the geomagnetic field. *Phys Earth Planet Inter* 13:245–259.
20. Smirnov AV, Kulakov EV, Foucher MS, Bristol KE (2017) Intrinsic paleointensity bias and the long-term history of the geodynamo. *Sci Adv* 3:e1602306.
21. Paterson GA (2011) A simple test for the presence of multidomain behaviour during paleointensity experiments. *J Geophys Res* 116:B10104.
22. Fabian K (2009) Thermochemical remanence acquisition in single-domain particle ensembles: A case for possible overestimation of the geomagnetic paleointensity. *Geochem Geophys Geosyst* 10:Q06Z03.
23. Zhao X, et al. (2014) The effects of secondary mineral formation on Coe-type paleointensity determinations: Theory and simulation. *Geochem Geophys Geosyst* 15: 1215–1234.
24. Gribov SK, Dolotov AV, Shcherbakov VP (2017) Experimental modeling of the chemical remanent magnetization and Thellier procedure on titanomagnetite-bearing basalts. *Izv Acad Sci USSR Phys Solid Earth* 53:274–292.
25. Day R, Fuller MD, Schmidt VA (1977) Hysteresis properties of titanomagnetites: Grain-size and compositional dependence. *Phys Earth Planet Inter* 13:260–267.
26. Dunlop DJ (2002) Theory and application of the Day plot (Mrs/Ms versus Hcr/Hc) 1. Theoretical curves and tests using titanomagnetite data. *J Geophys Res* 107: EPM 4-1–EPM 4-22.
27. Muxworthy AR, Williams W, Virdee D (2003) Effect of magnetostatic interactions on the hysteresis parameters of single-domain and pseudo-single-domain grains. *J Geophys Res* 108:2517.
28. Heslop D (2005) A Monte Carlo investigation of the representation of thermally activated single-domain particles within the Day plot. *Stud Geophys Geod* 49:163–176.
29. Frank U, Nowaczyk NR (2008) Mineral magnetic properties of artificial samples systematically mixed from haematite and magnetite. *Geophys J Int* 175:449–461.
30. Paterson GA, Biggin AJ, Hodgson E, Hill MJ (2015) Thellier-type paleointensity data from multidomain specimens. *Phys Earth Planet Inter* 245:117–133.
31. Calvo M, Prévot M, Perrin M, Riisager J (2002) Investigating the reasons for the failure of palaeointensity experiments: A study on historical lava flows from Mt. Etna (Italy). *Geophys J Int* 149:44–63.
32. Pike CR, Roberts AP, Verosub KL (1999) Characterizing interactions in fine magnetic particle systems using first order reversal curves. *J Appl Phys* 85:6660–6667.
33. Lascu I, et al. (2015) Magnetic unmixing of first-order reversal curve diagrams using principal component analysis. *Geochem Geophys Geosyst* 16:2900–2915.
34. Zhao X, et al. (2017) Magnetic domain state diagnosis using hysteresis reversal curves. *J Geophys Res* 122:4767–4789.
35. Coe RS (1967) Paleo-intensities of the Earth's magnetic field determined from Tertiary and Quaternary rocks. *J Geophys Res* 72:3247–3262.
36. Yu YJ, Tauxe L, Genevey A (2004) Toward an optimal geomagnetic field intensity determination technique. *Geochem Geophys Geosyst* 5:Q02H07.
37. Paterson GA, Heslop D, Pan Y (2016) The pseudo-Thellier palaeointensity method: New calibration and uncertainty estimates. *Geophys J Int* 207:1596–1608.
38. Yamamoto Y, Hoshi H (2008) Paleomagnetic and rock magnetic studies of the Sakurajima 1914 and 1946 andesitic lavas from Japan: A comparison of the LTD-DHT Shaw and Thellier paleointensity methods. *Phys Earth Planet Inter* 167:118–143.
39. Paterson GA, et al. (2010) Paleomagnetic determination of emplacement temperatures of pyroclastic deposits: An under-utilized tool. *Bull Volcanol* 72:309–330.
40. Muxworthy AR, Heslop D, Paterson GA, Michalk D (2011) A Preisach method for estimating absolute paleofield intensity under the constraint of using only isothermal measurements: 2. Experimental testing. *J Geophys Res* 116:B04103.
41. Muxworthy AR (1998) Stability of magnetic remanence in multidomain magnetite. PhD thesis (Univ Oxford, Oxford).
42. Jackson M, Solheid P (2010) On the quantitative analysis and evaluation of magnetic hysteresis data. *Geochem Geophys Geosyst* 11:Q04Z15.
43. Stoner EC, Wohlfarth EP (1948) A mechanism of magnetic hysteresis in heterogeneous alloys. *Philos Trans R Soc Lond A* 240:599–642.
44. Wohlfarth EP (1958) Relations between different modes of acquisition of the remanent magnetization of ferromagnetic particles. *J Appl Phys* 29:595–596.
45. Joffe I, Heubregbr R (1974) Hysteresis properties of distributions of cubic single-domain ferromagnetic particles. *Philos Mag* 29:1051–1059.
46. Xu H, Yang Z, Peng P, Meert JG, Zhu R (2014) Paleo-position of the North China craton within the supercontinent Columbia: Constraints from new paleomagnetic results. *Precambrian Res* 255:276–293.
47. Reshef DN, et al. (2011) Detecting novel associations in large data sets. *Science* 334: 1518–1524.

Supporting Information

Paterson et al. 10.1073/pnas.1714047114

SI Methods

The two principal components (PC1 and PC2) of the hysteresis data are given by

$$\begin{pmatrix} \text{PC1} \\ \text{PC2} \end{pmatrix} = \begin{pmatrix} -0.5231 & 0.8523 \\ 0.8523 & 0.5231 \end{pmatrix} \begin{pmatrix} \log_{10}(X) - 0.6062 \\ \log_{10}(Y) + 1.2018 \end{pmatrix}. \quad \textbf{[S1]}$$

BDS is defined as PC1/1.3414, where 1.3414 is PC1 for a single grain yielding a perfectly square hysteron ($B_{cr}/B_c = 1$, $M_{rs}/M_s = 1$).

SI Dataset Descriptions

A summary of the datasets used in this study is given in Table S1.

Sized Dataset. Refs. 1–34 are for the size (titano-) magnetite hysteresis data presented in Fig. 1 and given in Dataset S1. Specimens have been sourced from crushed natural magnetite (e.g., refs. 1, 7, and 10), have been chemically synthesized (e.g., refs. 15 and 16), or have been commercially purchased (e.g., refs. 27 and 34). All specimens have experienced various degrees of annealing, depending on the primary objective of each study.

Although the composition of the sized (titano-) magnetite ($Fe_{3-x}Ti_xO_4$) is not consistently reported, Ti concentrations have been reported to vary from x = 0 to x = 0.6 (2, 9). Variable degrees of aluminum substitution (e.g., refs. 7 and 9) as well as some possible (surficial) oxidation to maghemite (24, 27) have also been reported for specimens collated in this dataset.

Wang and Van der Voo (35) proposed trends in plots of M_{rs}/M_s versus B_c that could be related to magnetic grain size variations from different compositions of titanomagnetite. Their analysis suggested that high-Ti and low-Ti titanomagnetite would fall on two distinctive slopes. In Fig. S2*A*, we plot M_{rs}/M_s versus B_c for 273 specimens with B_c data from the Sized Dataset alongside the high-Ti and low-Ti trends of Wang and Van der Voo. The Sized Dataset predominantly falls between the trend lines, which indicates a range of titanium substitution values. We also note a distinct high coercivity slope at values ≥50 mT, which is above the range of values explored by Wang and Van der Voo. This suggests a nonlinear relationship, which should be expected given the theoretical upper bound of $M_{rs}/M_s = 0.86$ for an assemblage of identical grains with cubic magnetocrystalline anisotropy (36).

Geological Dataset. Refs. 35 and 37–95 are for the geological specimen hysteresis data presented in Fig. 1 and given in Dataset S2. This dataset contains 2,682 hysteresis data taken from 60 studies of geological materials that can be used for paleointensity study (paleointensity data are not collated for this dataset). Some hysteresis data from the Control and Historical Datasets are included in this dataset. Lithologically, this dataset consists of a range of intrusive and extrusive igneous rocks, including basalt, andesite, dacite, rhyolite, dolerite, and gabbro, as well as basaltic glasses and isolated single crystals of feldspar, among other rock types (Dataset S2). Compositional data have not been collated for this dataset, but (titano-) magnetite, maghemite, and hematite are reported (e.g., refs. 65, 69, 72, 76, and 83). M_{rs}/M_s versus B_c for a subset of 1,831 specimens with B_c data are shown in Fig. S2*B*. The geological specimens have a wide spread of values between the proposed compositional trends, which suggests a wide range of titanium substitution, if titanomagnetite is assumed to be the dominant carrier.

Archeological Dataset. Refs. 96–114 are for the archeological specimen hysteresis data presented in Fig. 1 and given in Dataset S3. This dataset contains 504 hysteresis data taken from 18 studies of archeological materials that can be used for archeointensity study (archeointensity data are not collated for this dataset). The specimens represent a range of materials, including bricks, burnt floors and walls, ceramics, clay, hearths, kilns, and pottery/potsherds. Compositional data have not been collated for this dataset, but (titano-) magnetite, maghemite, hematite, and possibly goethite are reported carriers in these specimens (e.g., refs. 100, 101, and 105). M_{rs}/M_s versus B_c is shown for a subset of 295 specimens with B_c data in Fig. S2*C*. The archeological specimens have a wide spread of values between the proposed compositional trends, which suggests a range of titanium substitution, if titanomagnetite is assumed to be the dominant carrier.

Control Dataset. This dataset consists of 162 specimens where magnetic hysteresis data can be associated with results from laboratory control paleointensity experiments. This includes a total of 151 thermally stabilized geological specimens (a mixture of basalt, intrusive bodies, and pyroclastic materials), which were subjected to new paleointensity and rock magnetic experiments. These specimens, which are from previous studies (61, 65, 72) and from unmeasured specimens, include pyroclastic lithic clasts (basalts, andesites, dacites, syenites, and leucite tephrites), flood basalts, intrusive dikes, granites, and granitoids. Unmeasured specimens are from the Emeishan Large Igneous Province and Permian mafic dikes from Yunnan and Sichuan Provinces, China, pink granites from Qingdao, China, and granitoids from Xinjiang Province, China. Eleven results are from sized magnetite (also in the Sized Dataset) that have both hysteresis and paleointensity data (19, 27). The M_{rs}/M_s versus B_{cr}/B_c plot for the Control Dataset is shown in Fig. S3*A*, where it is shown that BDS accounts for ∼97% of the dataset variance.

Rock magnetic data indicate the magnetic carriers are dominantly (titano-) magnetite and hematite (92), but detailed estimates of titanium substitution are not available (i.e., there are currently no Curie temperature estimates). M_{rs}/M_s versus B_c for the 151 geological specimens is shown in Fig. S2*D*. The control specimens tend to follow the low-Ti trend of Wang and Van der Voo (35), but also exhibit the high coercivity tail seen in the Sized Dataset. No B_c data are available for the 11 sized specimens.

Historical Dataset. This dataset consists of 129 specimens where magnetic hysteresis data can be associated with results from natural paleointensity experiments (i.e., the original magnetization was acquired in nature and not in the laboratory). The specimens include basalt, andesite, dacite, and pyroclastic lithics (basalts, andesites, dacites, syenites, and leucite tephrites) from Sakurajima, Japan (61); Mount St. Helens, United States (65); Láscar, Chile (65); Parícutin, Mexico (72); and Vesuvius, Italy (72).

The M_{rs}/M_s versus B_{cr}/B_c plot for the Historical Dataset is shown in Fig. S3*B*, where it is shown that BDS accounts for ∼94% of the dataset variance.

Curie temperature data indicate the titanomagnetite (x = 0.0 to 0.6) is the main magnetic mineral, but hematite is present in some pyroclastic lithics (61, 65, 72). M_{rs}/M_s versus B_c for these specimens is shown in Fig. S2*E* and suggests the low-Ti titanomagnetite is dominant. This is inconsistent with the Curie temperature data, but may be a result of mixed mineralogy.

SI Factors That Can Obscure BDS Relationships

Here we show how the number of data and using only a single paleointensity estimate per specimen can influence the ability to identify a relationship between BDS and paleointensity inaccuracy, using a Monte Carlo resampling of the 160 accepted specimens from the Control Dataset.

To explore the effect of number of specimens, we resample 20 to 160 specimens (without replacement) 10^4 times. For each resampling, we determine the MIC and associated P value for the relationship between BDS and paleointensity inaccuracy. We then calculate the proportion of resamplings where we cannot reject the null hypothesis that there is no correlation at the 5% significance level. This analysis indicates that at least ∼100 specimens are needed to consistently identify a significant relationship (Fig. S4*A*). With fewer specimens, the relationship between BDS and paleointensity inaccuracy is unlikely to be clearly identified.

To explore the effect of selecting a single Arai plot fit per specimen, for each specimen, we randomly select one acceptable fit for 20 to 160 specimens (without replacement). This is repeated 10^4 times for each number of resampled specimens. Selecting a single Arai plot fit per specimen fails to consistently identify the BDS and paleointensity inaccuracy relationship, irrespective of how many specimens are used (Fig. S4*B*). Even when all 160 specimens are used, there is a less than 40% chance of identifying the relationship, which can be attributed to failure to characterize the specimens' general paleointensity behavior with just a single Arai plot fit.

Site level heterogeneity may also influence the ability to identify a clear relation if the paleointensity and hysteresis data are not intimately associated. In Fig. S4*C*, we present the distributions of BDS at the site level for basaltic and andesitic lava flows from studies in refs. 61 and 72. Although some sites exhibit narrow ranges of BDS, others are much more scattered, and this may yield insignificant relationships if paleointensity and hysteresis data are not intimately associated.

1. Parry L (1975) Magnetization of micron sized magnetite particles. *Aust J Phys* 28:693–706.
2. Day R, Fuller MD, Schmidt VA (1977) Hysteresis properties of titanomagnetites: Grain-size and compositional dependence. *Phys Earth Planet Inter* 13:260–267.
3. Levi S, Merrill RT (1978) Properties of single-domain, pseudo-single-domain, and multidomain magnetite. *J Geophys Res* 83:309–323.
4. Parry LG (1979) Magnetization of multidomain particles of magnetite. *Phys Earth Planet Inter* 19:21–30.
5. Parry LG (1980) Shape-related factors in the magnetization of immobilized magnetite particles. *Phys Earth Planet Inter* 22:144–154.
6. Dankers P, Sugiura N (1981) The effects of annealing and concentration on the hysteresis properties of magnetite around the PSD-MD transition. *Earth Planet Sci Lett* 56:422–428.
7. Hartstra RL (1982) Grain-size dependence of initial susceptibility and saturation magnetization-related parameters of four natural magnetites in the PSD–MD range. *Geophys J R Astron Soc* 71:477–495.
8. Özdemir Ö, Banerjee SK (1982) A preliminary magnetic study of soil samples from west-central Minnesota. *Earth Planet Sci Lett* 59:393–403.
9. Özdemir Ö, O'Reilly W (1982) An experimental study of the intensity and stability of thermoremanent magnetization acquired by synthetic monodomain titanomagnetite substituted by aluminium. *Geophys J R Astron Soc* 70:141–154.
10. Bailey ME, Dunlop DJ (1983) Alternating field characteristics of pseudo-single-domain (2–14 μm) and multidomain magnetite. *Earth Planet Sci Lett* 63:335–352.
11. Dunlop DJ (1983) Viscous magnetization of 0.04–100 μm magnetites. *Geophys J R Astron Soc* 74:667–687.
12. Dunlop DJ (1986) Hysteresis properties of magnetite and their dependence on particle size: A test of pseudo-single-domain remanence models. *J Geophys Res* 91:9569–9584.
13. Schmidbauer E, Schembera N (1987) Magnetic hysteresis properties and anhysteretic remanent magnetization of spherical Fe_3O_4 particles in the grain size range 60–160 nm. *Phys Earth Planet Inter* 46:77–83.
14. Argyle KS, Dunlop DJ (1990) Low-temperature and high-temperature hysteresis of small multidomain magnetites (215–540 nm). *J Geophys Res* 95:7069–7082.
15. Heider F, Zitzelsberger A, Fabian K (1996) Magnetic susceptibility and remanent coercive force in grown magnetite crystals from 0.1 μm to 6 mm. *Phys Earth Planet Inter* 93:239–256.
16. Schmidbauer E, Keller R (1996) Magnetic properties and rotational hysteresis of Fe_3O_4 and γ-Fe_2O_3 particles ∼ 250 nm in diameter. *J Magn Magn Mater* 152:99–108.
17. Özdemir Ö, Dunlop DJ (1997) Effect of crystal defects and internal stress on the domain structure and magnetic properties of magnetite. *J Geophys Res* 102:20211–20224.
18. Özdemir Ö, Dunlop DJ (1998) Single-domain-like behavior in a 3-mm natural single crystal of magnetite. *J Geophys Res* 103:2549–2562.
19. Muxworthy AR (1998) Stability of magnetic remanence in multidomain magnetite. PhD thesis (Univ Oxford, Oxford).
20. Muxworthy AR (1999) Low-temperature susceptibility and hysteresis of magnetite. *Earth Planet Sci Lett* 169:51–58.
21. Shcherbakova VV, Shcherbakov VP, Heider F (2000) Properties of partial thermoremanent magnetization in pseudosingle domain and multidomain magnetite grains. *J Geophys Res* 105:767–781.
22. Kosterov A (2001) Magnetic hysteresis of pseudo-single-domain and multidomain magnetite below the Verwey transition. *Earth Planet Sci Lett* 186:245–253.
23. Dunlop DJ (2002) Theory and application of the day plot (M_{rs}/M_s versus H_{cr}/H_c) 1. Theoretical curves and tests using titanomagnetite data. *J Geophys Res* 107:EPM 4-1–EPM 4-22.
24. Muxworthy AR, Dunlop DJ (2002) First-order reversal curve (FORC) diagrams for pseudo-single-domain magnetites at high temperature. *Earth Planet Sci Lett* 203:369–382.
25. Özdemir Ö, Dunlop DJ, Moskowitz BM (2002) Changes in remanence, coercivity and domain state at low temperature in magnetite. *Earth Planet Sci Lett* 194:343–358.
26. Yu Y, Dunlop DJ, Özdemir Ö (2002) Partial anhysteretic remanent magnetization in magnetite 1. Additivity. *J Geophys Res* 107:2244.
27. Krása D, Heunemann C, Leonhardt R, Petersen N (2003) Experimental procedure to detect multidomain remanence during Thellier-Thellier experiments. *Phys Chem Earth* 28:681–687.
28. Muxworthy AR, Williams W (2006) Low-temperature viscous magnetization of multidomain magnetite: Evidence for disaccommodation contribution. *J Magn Magn Mater* 307:113–119.
29. Muxworthy AR, Williams W (2006) Observations of viscous magnetization in multidomain magnetite. *J Geophys Res* 111:B01103.
30. Krása D, et al. (2009) Nanofabrication of two-dimensional arrays of magnetite particles for fundamental rock magnetic studies. *J Geophys Res* 114:B02104.
31. Smirnov AV (2009) Grain size dependence of low-temperature remanent magnetization in natural and synthetic magnetite: Experimental study. *Earth Planets Space* 61:119–124.
32. Krása D, Muxworthy AR, Williams W (2011) Room- and low-temperature magnetic properties of 2-D magnetite particle arrays. *Geophys J Int* 185:167–180.
33. Biggin AJ, et al. (2013) The effect of cooling rate on the intensity of thermoremanent magnetization (TRM) acquired by assemblages of pseudo-single domain, multidomain and interacting single-domain grains. *Geophys J Int* 193:1239–1249.
34. Almeida TP, et al. (2015) Effect of maghemization on the magnetic properties of nonstoichiometric pseudo-single-domain magnetite particles. *Geochem Geophys Geosyst* 16:2969–2979.
35. Wang D, Van der Voo R (2004) The hysteresis properties of multidomain magnetite and titanomagnetite/titanomaghemite in mid-ocean ridge basalts. *Earth Planet Sci Lett* 220:175–184.
36. Joffe I, Heubregbr R (1974) Hysteresis properties of distributions of cubic single-domain ferromagnetic particles. *Philos Mag* 29:1051–1059.
37. Mandeville CW, Carey S, Sigurdsson H, King J (1994) Paleomagnetic evidence for high-temperature emplacement of the 1883 subaqueous pyroclastic flows from Krakatau Volcano, Indonesia. *J Geophys Res* 99:9487–9504.
38. Gonzalez S, Sherwood G, Böhnel H, Schnepp E (1997) Palaeosecular variation in Central Mexico over the last 30,000 years: The record from lavas. *Geophys J Int* 130:201–219.
39. Rolph TC (1997) An investigation of the magnetic variation within two recent lava flows. *Geophys J Int* 130:125–136.
40. Johnson CL, et al. (1998) Ar-40/Ar-39 ages and paleomagnetism of Sao Miguel lavas, Azores. *Earth Planet Sci Lett* 160:637–649.
41. Kosterov AA, Perrin M, Glen JM, Coe RS (1998) Paleointensity of the Earth's magnetic field in early Cretaceous time: The Paraná Basalt, Brazil. *J Geophys Res* 103:9739–9753.
42. Kosterov AA, Prévot M (1998) Possible mechanisms causing failure of Thellier palaeointensity experiments in some basalts. *Geophys J Int* 134:554–572.
43. Hill MJ, Shaw J (1999) Palaeointensity results for historic lavas from Mt Etna using microwave demagnetization/remagnetization in a modified Thellier-type experiment. *Geophys J Int* 139:583–590.
44. Hill MJ, Shaw J (2000) Magnetic field intensity study of the 1960 Kilauea lava flow, Hawaii, using the microwave palaeointensity technique. *Geophys J Int* 142:487–504.
45. Calvo M, Prévot M, Perrin M, Riisager J (2002) Investigating the reasons for the failure of palaeointensity experiments: A study on historical lava flows from Mt. Etna (Italy). *Geophys J Int* 149:44–63.
46. Hill MJ, Gratton MN, Shaw J (2002) A comparison of thermal and microwave palaeomagnetic techniques using lava containing laboratory induced remanence. *Geophys J Int* 151:157–163.
47. Biggin AJ, Thomas DN (2003) The application of acceptance criteria to results of Thellier palaeointensity experiments performed on samples with pseudo-single-domain-like characteristics. *Phys Earth Planet Inter* 138:279–287.
48. Carvallo C, Camps P, Ruffet G, Henry B, Poidras T (2003) Mono Lake or Laschamp geomagnetic event recorded from lava flows in Amsterdam Island (southeastern Indian Ocean). *Geophys J Int* 154:767–782.
49. Smirnov AV, Tarduno JA (2003) Magnetic hysteresis monitoring of Cretaceous submarine basaltic glass during Thellier paleointensity experiments: Evidence for alteration and attendant low field bias. *Earth Planet Sci Lett* 206:571–585.

50. Smirnov AV, Tarduno JA, Pisakin BN (2003) Paleointensity of the early geodynamo (2.45 Ga) as recorded in Karelia: A single-crystal approach. *Geology* 31:415–418.
51. Carvallo C, Özdemir Ö, Dunlop DJ (2004) Palaeointensity determinations, palaeodirections and magnetic properties of basalts from the Emperor seamounts. *Geophys J Int* 156:29–38.
52. Coe RS, Leonhardt R, Krása D, Riisager J, Plenier G (2004) Multidomain behavior during Thellier paleointensity experiments: Results from the 1915 Mt. Lassen flow. *Phys Earth Planet Inter* 147:141–153.
53. McArdle NJ, Halls HC, Shaw J (2004) Rock magnetic studies and a comparison between microwave and Thellier palaeointensities for Canadian Precambrian dykes. *Phys Earth Planet Inter* 147:247–254.
54. Nakamura N, Iyeda Y (2005) Magnetic properties and paleointensity of pseudotachylytes from the Sudbury structure, Canada: Petrologic control. *Tectonophysics* 402:141–152.
55. Smirnov AV, Tarduno JA (2005) Thermochemical remanent magnetization in Precambrian rocks: Are we sure the geomagnetic field was weak? *J Geophys Res* 110:B06103.
56. Wehland F, Leonhardt R, Vadeboin F, Appel E (2005) Magnetic interaction analysis of basaltic samples and pre-selection for absolute palaeointensity measurements. *Geophys J Int* 162:315–320.
57. Bowles J, et al. (2006) Paleointensity applications to timing and extent of eruptive activity, 9°–10°N East Pacific Rise. *Geochem Geophys Geosyst* 7:Q06006.
58. Goguitchaichvili A, et al. (2007) Paleomagnetism of the Eastern Alkaline Province (Mexico): Contribution to the time-averaged field global database and geomagnetic instability time scale. *Earth Planets Space* 59:775–783.
59. Pressling N, Brown MC, Gratton MN, Shaw J, Gubbins D (2007) Microwave palaeointensities from Holocene age Hawaiian lavas: Investigation of magnetic properties and comparison with thermal palaeointensities. *Phys Earth Planet Inter* 162:99–118.
60. Cottrell RD, Tarduno JA, Roberts J (2008) The Kiaman Reversed Polarity Superchron at Kiama: Toward a field strength estimate based on single silicate crystals. *Phys Earth Planet Inter* 169:49–58.
61. Yamamoto Y, Hoshi H (2008) Paleomagnetic and rock magnetic studies of the Sakurajima 1914 and 1946 andesitic lavas from Japan: A comparison of the LTD-DHT Shaw and Thellier paleointensity methods. *Phys Earth Planet Inter* 167:118–143.
62. Miki M, et al. (2009) Palaeomagnetism and geochronology of the Proterozoic dolerite dyke from southwest Greenland: Indication of low palaeointensity*. *Geophys J Int* 179:18–34.
63. Tanaka H, Komuro N (2009) The Shaw paleointensity method: Can the ARM simulate the TRM alteration? *Phys Earth Planet Inter* 173:269–278.
64. Ferk A, Aulock FWv, Leonhardt R, Hess K-U, Dingwell DB (2010) A cooling rate bias in paleointensity determination from volcanic glass: An experimental demonstration. *J Geophys Res* 115:B08102.
65. Paterson GA, Muxworthy AR, Roberts AP, Mac Niocaill C (2010) Assessment of the usefulness of lithic clasts from pyroclastic deposits for paleointensity determination. *J Geophys Res* 115:B03104.
66. Spassov S, et al. (2010) Rock magnetic property and paleointensity determination on historical Santorini lava flows. *Geochem Geophys Geosyst* 11:Q07006.
67. Yamamoto Y, Shibuya H, Tanaka H, Hoshizumi H (2010) Geomagnetic paleointensity deduced for the last 300 kyr from Unzen Volcano, Japan, and the dipolar nature of the Iceland Basin excursion. *Earth Planet Sci Lett* 293:236–249.
68. Calvo-Rathert M, et al. (2011) A paleomagnetic and paleointensity study on Pleistocene and Pliocene basaltic flows from the Djavakheti Highland (Southern Georgia, Caucasus). *Phys Earth Planet Inter* 187:212–224.
69. Donadini F, Elming S-A, Tauxe L, Halenius U (2011) Paleointensity determination on a 1.786 Ga old gabbro from Hoting, Central Sweden. *Earth Planet Sci Lett* 309:234–248.
70. Kissel C, et al. (2011) The Mono Lake excursion recorded in phonolitic lavas from Tenerife (Canary Islands): Paleomagnetic analyses and coupled K/Ar and Ar/Ar dating. *Phys Earth Planet Inter* 187:232–244.
71. Mena M, Goguitchaichvili A, Solano MC, Vilas JF (2011) Paleosecular variation and absolute geomagnetic paleointensity records retrieved from the Early Cretaceous Posadas Formation (Misiones, Argentina). *Stud Geophys Geod* 55:279.
72. Muxworthy AR, Heslop D, Paterson GA, Michalk D (2011) A Preisach method for estimating absolute paleofield intensity under the constraint of using only isothermal measurements: 2. Experimental testing. *J Geophys Res* 116:B04103.
73. Ferk A, et al. (2012) Paleointensity on volcanic glass of varying hydration states. *Phys Earth Planet Inter* 208:25–37.
74. Koch SA, Gilder SA, Pohl J, Trepmann C (2012) Geomagnetic field intensity recorded after impact in the Ries meteorite crater, Germany. *Geophys J Int* 189:383–390.
75. Shcherbakova VV, Bakhmutov VG, Shcherbakov VP, Zhidkov GV, Shpyra VV (2012) Palaeointensity and palaeomagnetic study of Cretaceous and Palaeocene rocks from Western Antarctica. *Geophys J Int* 189:204–228.
76. Calvo-Rathert M, et al. (2013) Rock-magnetic and paleomagnetic results from the Tepic-Zacoalco rift region (western Mexico). *Stud Geophys Geod* 57:309–331.
77. Muxworthy AR, Evans ME (2013) Micromagnetics and magnetomineralogy of ultrafine magnetite inclusions in the Modipe Gabbro. *Geochem Geophys Geosyst* 14:921–928.
78. Wang H, Kent DV (2013) A paleointensity technique for multidomain igneous rocks. *Geochem Geophys Geosyst* 14:4195–4213.
79. Bowles JA, et al. (2014) Eruptive timing and 200 year episodicity at 92°W on the hot spot-influenced Galapagos Spreading Center derived from geomagnetic paleointensity. *Geochem Geophys Geosyst* 15:2211–2224.
80. Kissel C, et al. (2014) A combined paleomagnetic/dating investigation of the upper Jaramillo transition from a volcanic section at Tenerife (Canary Islands). *Earth Planet Sci Lett* 406:59–71.
81. Konstantinov KM, Bazhenov ML, Fetisova AM, Khutorskoy MD (2014) Paleomagnetism of trap intrusions, East Siberia: Implications to flood basalt emplacement and the Permo-Triassic crisis of biosphere. *Earth Planet Sci Lett* 394:242–253.
82. Roperch P, Chauvin A, Le Pennec J-L, Lara LE (2014) Paleomagnetic study of juvenile basaltic-andesite clasts from Andean pyroclastic density current deposits. *Phys Earth Planet Inter* 227:20–29.
83. Xu H, Yang Z, Peng P, Meert JG, Zhu R (2014) Paleo-position of the North China craton within the supercontinent Columbia: Constraints from new paleomagnetic results. *Precambrian Res* 255:276–293.
84. Bono RK, Tarduno JA (2015) A stable Ediacaran Earth recorded by single silicate crystals of the ca. 565 Ma Sept-Îles intrusion. *Geology* 43:131–134.
85. Bowles JA, Gee JS, Jackson MJ, Avery MS (2015) Geomagnetic paleointensity in historical pyroclastic density currents: Testing the effects of emplacement temperature and postemplacement alteration. *Geochem Geophys Geosyst* 16:3607–3625.
86. Dodd SC, Mac Niocaill C, Muxworthy AR (2015) Long duration (>4 Ma) and steady-state volcanic activity in the early Cretaceous Paraná–Etendeka Large Igneous Province: New palaeomagnetic data from Namibia. *Earth Planet Sci Lett* 414:16–29.
87. Dodd SC, Muxworthy AR, Mac Niocaill C (2015) Paleointensity determinations from the Etendeka province, Namibia, support a low-magnetic field strength leading up to the Cretaceous normal superchron. *Geochem Geophys Geosyst* 16:785–797.
88. Kissel C, et al. (2015) Holocene geomagnetic field intensity variations: Contribution from the low latitude Canary Islands site. *Earth Planet Sci Lett* 430:178–190.
89. Smirnov AV, Evans DAD (2015) Geomagnetic paleointensity at ∼2.41 Ga as recorded by the Widgiemooltha Dike Swarm, Western Australia. *Earth Planet Sci Lett* 416:35–45.
90. Usui Y, Shibuya T, Sawaki Y, Komiya T (2015) Rock magnetism of tiny exsolved magnetite in plagioclase from a Paleoarchean granitoid in the Pilbara craton. *Geochem Geophys Geosyst* 16:112–125.
91. Calvo-Rathert M, Morales-Contreras J, Carrancho Á, Goguitchaichvili A (2016) A comparison of Thellier-type and multispecimen paleointensity determinations on Pleistocene and historical lava flows from Lanzarote (Canary Islands, Spain). *Geochem Geophys Geosyst* 17:3638–3654.
92. Paterson GA, Heslop D, Pan Y (2016) The pseudo-Thellier palaeointensity method: New calibration and uncertainty estimates. *Geophys J Int* 207:1596–1608.
93. Carvallo C (2017) Data report: hysteresis properties of igneous rocks from Holes U1439C, U1440B, and U1442A. *Izu-Bonin-Mariana Fore Arc Proceedings of the International Ocean Discovery Program*, eds Reagan MK, Pearce JA, Petronotis KE, the Expedition 352 Scientists (Int Ocean Discovery Program, College Station, TX), Vol 352.
94. Kapper L, et al. (2017) A paleointensity study of Cretaceous volcanic rocks from the Western Cordillera, Colombia. *Stud Geophys Geod* 61:264–289.
95. Usui Y, Tian W (2017) Paleomagnetic directional groups and paleointensity from the flood basalt in the Tarim large igneous province: Implications for eruption frequency. *Earth Planets Space* 69:14.
96. Cui YL, Verosub KL, Roberts AP, Kovacheva M (1997) Mineral magnetic studies of archaeological samples: Implications for sample selection for paleointensity determinations. *J Geomag Geoelectr* 49:567–585.
97. Shaw J, Yang S, Rolph TC, Sun FY (1999) A comparison of archaeointensity results from Chinese ceramics using microwave and conventional Thellier's and Shaw's methods. *Geophys J Int* 136:714–718.
98. Yu Y, Dunlop DJ, Pavlish L, Cooper M (2000) Archeomagnetism of Ontario potsherds from the last 2000 years. *J Geophys Res* 105:19419–19433.
99. Donadini F, Kovacheva M, Kostadinova M, Casas L, Pesonen LJ (2007) New archaeointensity results from Scandinavia and Bulgaria: Rock-magnetic studies inference and geophysical application. *Phys Earth Planet Inter* 165:229–247.
100. Herries AIR, Kovacheva M, Kostadinova M, Shaw J (2007) Archaeo-directional and -intensity data from burnt structures at the Thracian site of Halka Bunar (Bulgaria): The effect of magnetic mineralogy, temperature and atmosphere of heating in antiquity. *Phys Earth Planet Inter* 162:199–216.
101. Hill MJ, Lanos P, Chauvin A, Vitali D, Laubenheimer F (2007) An archaeomagnetic investigation of a Roman amphorae workshop in Albinia (Italy). *Geophys J Int* 169:471–482.
102. Hill MJ, Lanos P, Denti M, Dufresne P (2008) Archaeomagnetic investigation of bricks from the VIIIth–VIIth century BC Greek–indigenous site of Incoronata (Metaponto, Italy). *Phys Chem Earth* 33:523–533.
103. Rodriguez Ceja M, et al. (2009) Integrated archeomagnetic and micro–Raman spectroscopy study of pre-Columbian ceramics from the Mesoamerican formative village of Cuanalan, Teotihuacan Valley, Mexico. *J Geophys Res* 114:B04103.
104. Shaar R, et al. (2010) Testing the accuracy of absolute intensity estimates of the ancient geomagnetic field using copper slag material. *Earth Planet Sci Lett* 290:201–213.
105. McIntosh G, Kovacheva M, Catanzariti G, Donadini F, Lopez MLO (2011) High coercivity remanence in baked clay materials used in archeomagnetism. *Geochem Geophys Geosyst* 12:Q02003.
106. Morales J, et al. (2011) Are ceramics and bricks reliable absolute geomagnetic intensity carriers? *Phys Earth Planet Inter* 187:310–321.
107. Catanzariti G, et al. (2012) New archaeomagnetic data recovered from the study of Roman and Visigothic remains from central Spain (3rd-7th centuries). *Geophys J Int* 188:979–993.
108. Neukirch LP, et al. (2012) An archeomagnetic analysis of burnt grain bin floors from ca. 1200 to 1250 AD Iron-Age South Africa. *Phys Earth Planet Inter* 190–191:71–79.
109. Fanjat G, et al. (2013) First archeointensity determinations on Maya incense burners from Palenque temples, Mexico: New data to constrain the Mesoamerica secular variation curve. *Earth Planet Sci Lett* 363:168–180.

110. Gómez-Paccard M, Beamud E, McIntosh G, Larrasoaña JC (2013) New archaeomagnetic data recovered from the study of three Roman kilns from north-east Spain: A contribution to the Iberian palaeosecular variation curve. *Archaeometry* 55:159–177.
111. Kapper KL, Donadini F, Hirt AM (2015) Holocene archeointensities from mid European ceramics, slags, burned sediments and cherts. *Phys Earth Planet Inter* 241: 21–36.
112. Osete ML, et al. (2015) First archaeomagnetic field intensity data from Ethiopia, Africa (1615±12AD). *Phys Earth Planet Inter* 242:24–35.
113. Shaar R, et al. (2015) Decadal-scale variations in geomagnetic field intensity from ancient Cypriot slag mounds. *Geochem Geophys Geosyst* 16:195–214.
114. Carrancho Á, et al. (2017) Full-vector archaeomagnetic dating of a medieval limekiln at Pinilla Del Valle Site (Madrid, Spain). *Archaeometry* 59:373–394.

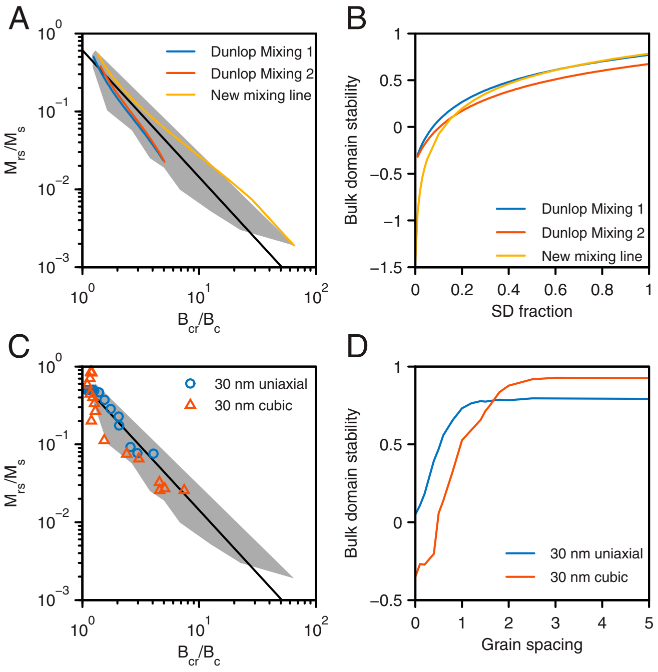

Fig. S1. Grain size mixing and interaction effects of BDS. (*A*) Hysteresis data for grain size mixing lines (1) and (*B*) mixing fraction relation with BDS. The new mixing line is derived from data from refs. 2 and 3. (*C*) Hysteresis data for models of interacting SD magnetite (4) and (*D*) modeled grain size spacing relation with BDS. The gray shaded areas in *A* and *C* represent the sized magnetite data cloud (Fig. 1*A*).

1. Dunlop DJ (2002) Theory and application of the day plot (M_{rs}/M_s versus H_{cr}/H_c) 1. Theoretical curves and tests using titanomagnetite data. *J Geophys Res* 107:EPM 4-1–EPM 4-22.
2. Heider F, Zitzelsberger A, Fabian K (1996) Magnetic susceptibility and remanent coercive force in grown magnetite crystals from 0.1 μm to 6 mm. *Phys Earth Planet Inter* 93:239–256.
3. Krása D, Muxworthy AR, Williams W (2011) Room- and low-temperature magnetic properties of 2-D magnetite particle arrays. *Geophys J Int* 185:167–180.
4. Muxworthy AR, Williams W, Virdee D (2003) Effect of magnetostatic interactions on the hysteresis parameters of single-domain and pseudo-single-domain grains. *J Geophys Res* 108:2517.

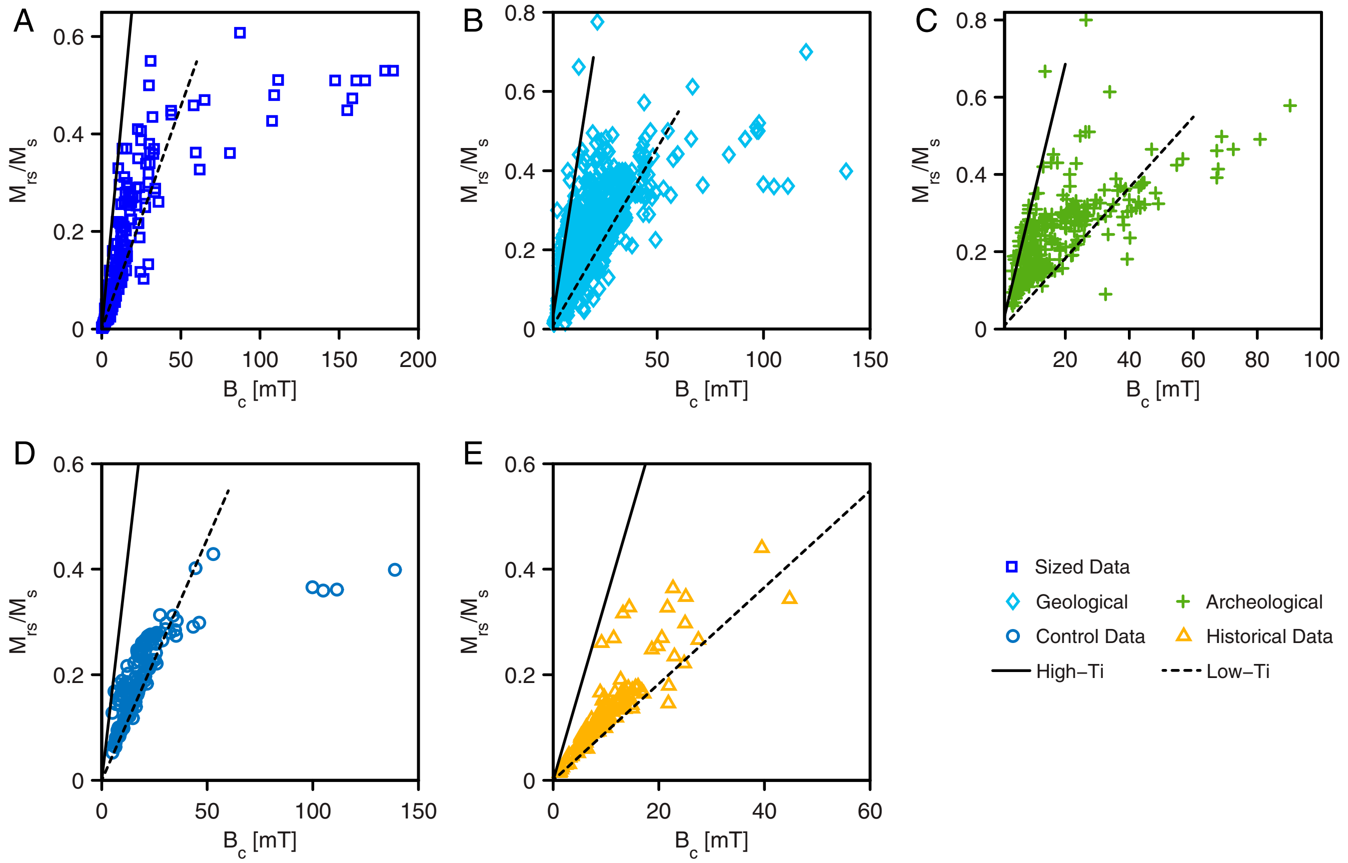

Fig. S2. M_{rs}/M_s versus B_c as a proxy for titanium content for titanomagnetite. Plots are shown for subsets of the (*A*) Sized Dataset (n = 273), (*B*) Geological Dataset (n = 1,831), (*C*) Archeological Dataset (n = 295), (*D*) Control Dataset (n = 151), and (*E*) the entire Historical Dataset (n = 129). In all plots, the solid and dashed black lines represent the high- and low-titanium trend lines, respectively, of ref. 1.

1. Wang D, Van der Voo R (2004) The hysteresis properties of multidomain magnetite and titanomagnetite/titanomaghemite in mid-ocean ridge basalts. *Earth Planet Sci Lett* 220: 175–184.

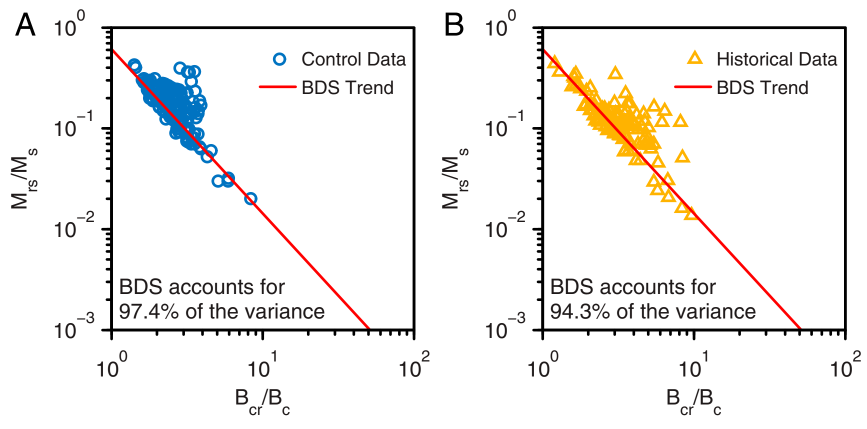

Fig. S3. PCA of hysteresis data. Hysteresis data and BDS trend for (*A*) the 160 accepted laboratory control and (*B*) the 112 accepted historical specimens.

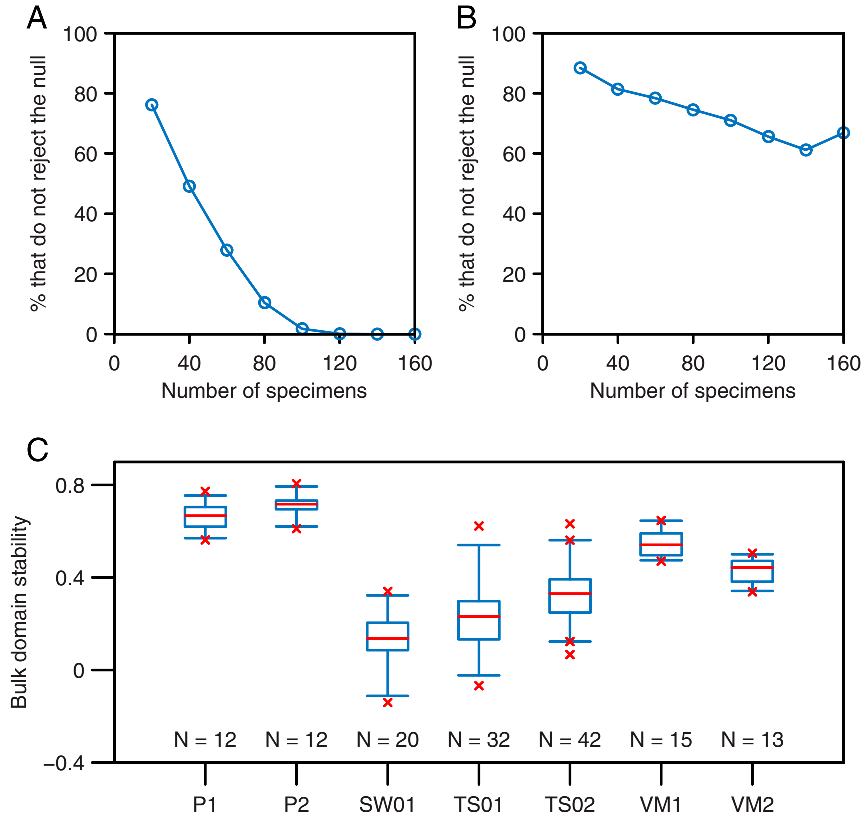

Fig. S4. The influence of data analyses on the ability to identify significant relations between rock magnetic properties and paleointensity results. (*A*) The proportion of results that fail to identify a significant relationship between BDS and paleointensity inaccuracy as a function of the number of specimens used. When less than ~80 to 100 specimens are used, a significant relationship may be missed. (*B*) The proportion of results that fail to identify a significant relationship between BDS and paleointensity inaccuracy when only a single paleointensity fit is made to each specimen as a function of the number of specimens used. Even when all 160 specimens are used, there is less than a 40% chance of identifying a significant relation. (*C*) Heterogeneity of BDS at the site level. When site level hysteresis is diverse (e.g., sites SW01, TS01, and TS02), associating paleointensity results with hysteresis data at the site level may obscure the relationships between BDS and paleointensity behavior. In *C*, the boxes denote the IQRs, the whiskers denote the 95% ranges, and the red lines are the median values. The red crosses represent values that lie outside the 95% ranges. Sites P1 and P2 are from Parícutin, Mexico (1); SW01, TS01, and TS02 are from Sakurajima, Japan (2); and VM1 and VM2 are from Vesuvius, Italy (1).

1. Muxworthy AR, Heslop D, Paterson GA, Michalk D (2011) A Preisach method for estimating absolute paleofield intensity under the constraint of using only isothermal measurements: 2. Experimental testing. *J Geophys Res* 116:B04103.
2. Yamamoto Y, Hoshi H (2008) Paleomagnetic and rock magnetic studies of the Sakurajima 1914 and 1946 andesitic lavas from Japan: A comparison of the LTD-DHT Shaw and Thellier paleointensity methods. *Phys Earth Planet Inter* 167:118–143.

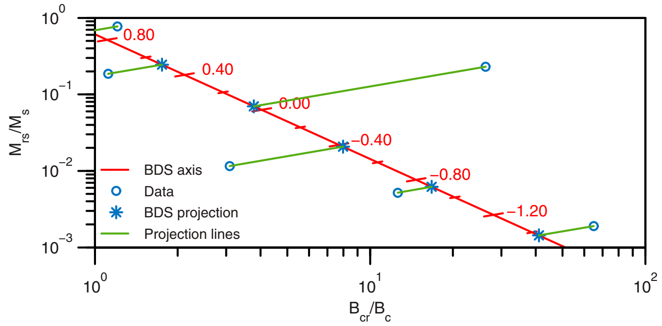

Fig. S5. Visual example of hysteresis data projected onto the BDS trend line. Hysteresis data are projected onto the BDS trend line using Eq. **1**. Red tick labels correspond to the BDS values of the ticks.

Table S1. Summary description of the datasets used in this study

Dataset name	Description	No. of specimens	Hysteresis data	Paleointensity data
Sized	Compilation of hysteresis data from (titano-) magnetite specimens with known grain size	303	Yes	No
Geological	Compilation of hysteresis data from geological materials typically used for paleointensity study; includes some data from the Control and Historical Datasets	2,682	Yes	No
Archeological	Compilation of hysteresis data from archeological materials typically used for archeointensity study	504	Yes	No
Control	New and published hysteresis and paleointensity data from laboratory control experiments; contains 11 specimens from the Sized Dataset; two paleointensity specimens rejected for analysis	162	Yes	Yes
Historic	Published hysteresis and paleointensity data from historical specimens, where he true paleointensity is known; 17 paleointensity specimens rejected for analysis	129	Yes	Yes
Combined	The Control and Historical Datasets combined; 19 paleointensity specimens rejected for analysis	291	Yes	Yes

Table S2. MIC for the relationships between various hysteresis quantifications and paleointensity selection statistics

	Control (n = 160)		Historical (n = 112)		Combined (n = 272)	
Statistic	MIC	P	MIC	P	MIC	P
B_{cr}/B_c						
$\lvert k' \rvert$	0.255	>0.060	0.291	>0.060	0.221	>0.060
δCK	0.233[†]	>0.060[†]	0.270	>0.060	0.188[‡]	>0.060[‡]
DRAT	0.227[†]	>0.060[†]	0.196	>0.060	0.186[‡]	>0.060[‡]
CDRAT	0.252[†]	>0.060[†]	0.193	>0.060	0.225[‡]	>0.060[‡]
DRATS	0.239[†]	>0.060[†]	0.158	>0.060	0.238[‡]	0.040[‡]
Mean DRAT	0.242[†]	>0.060[†]	0.183	>0.060	0.189[‡]	>0.060[‡]
δpal	0.256[†]	>0.060[†]	0.176	>0.060	0.172[‡]	>0.060[‡]
δTR	0.226	>0.060	0.302	>0.060	0.224	>0.060
$DRAT_{tail}$	0.276	>0.060	0.260	>0.060	*0.270*	*0.002*
MD_{vds}	0.238	>0.060	0.268	>0.060	0.231	>0.060
δt*	0.206	>0.060	0.252	>0.060	0.179	>0.060
Inaccuracy	0.250	>0.060	0.261	>0.060	0.219	>0.060
M_{rs}/M_s						
$\lvert k' \rvert$	*0.420*	*<0.001*	0.276	>0.060	*0.243*	*0.024*
δCK	*0.431*[†]	*<0.001*[†]	0.220	>0.060	*0.294*[‡]	*<0.001*[‡]
DRAT	*0.423*[†]	*<0.001*[†]	0.234	>0.060	*0.278*[‡]	*<0.001*[‡]
CDRAT	*0.314*[†]	*0.006*[†]	0.183	>0.060	*0.308*[‡]	*<0.001*[‡]
DRATS	*0.302*[†]	*0.013*[†]	0.170	>0.060	*0.313*[‡]	*<0.001*[‡]
Mean DRAT	*0.319*[†]	*0.004*[†]	0.223	>0.060	*0.237*[‡]	*0.043*[‡]
δpal	*0.403*[†]	*<0.001*[†]	0.208	>0.060	*0.338*[‡]	*<0.001*[‡]
δTR	*0.296*	*0.016*	0.237	>0.060	*0.248*	*0.015*
$DRAT_{tail}$	*0.347*	*<0.001*	0.266	>0.060	*0.258*	*0.006*
MD_{vds}	*0.362*	*<0.001*	0.262	>0.060	*0.260*	*0.005*
δt*	*0.389*	*<0.001*	0.277	>0.060	*0.281*	*<0.001*
Inaccuracy	*0.426*	*<0.001*	0.257	>0.060	*0.321*	*<0.001*
BDS						
$\lvert k' \rvert$	*0.389*	*<0.001*	*0.311*	*0.040*	*0.236*	*0.046*
δCK	*0.329*[†]	*0.002*[†]	0.283	>0.060	*0.274*[‡]	*0.001*[‡]
DRAT	*0.335*[†]	*0.001*[†]	*0.307*	*0.046*	*0.252*[‡]	*0.011*[‡]
CDRAT	*0.326*[†]	*0.003*[†]	0.237	>0.060	*0.290*[‡]	*<0.001*[‡]
DRATS	*0.335*[†]	*0.001*[†]	0.256	>0.060	*0.291*[‡]	*<0.001*[‡]
Mean DRAT	0.268[†]	>0.060[†]	0.196	>0.060	0.227[‡]	>0.060[‡]
δpal	*0.354*[†]	*<0.001*[†]	0.225	>0.060	*0.305*[‡]	*<0.001*[‡]
δTR	0.264	>0.060	0.234	>0.060	0.227	>0.060
$DRAT_{tail}$	0.263	>0.060	0.285	>0.060	0.227	>0.060
MD_{vds}	*0.302*	*0.011*	0.260	>0.060	*0.244*	*0.022*
δt*	*0.321*	*0.003*	0.301	>0.060	0.232	>0.060
Inaccuracy	*0.378*	*<0.001*	*0.309*	*0.042*	*0.324*	*<0.001*

Selection statistic definitions are given in ref. 1. MIC varies between 0 and 1. P values $\leq$ 0.05 are considered significant and are italicized.

[†]Here n = 158.

[‡]Here n = 270.

1. Paterson GA, Tauxe L, Biggin AJ, Shaar R, Jonestrask LC (2014) On improving the selection of Thellier-type paleointensity data. *Geochem Geophys Geosyst* 15:1180–1192.

Table S3. MIC for the relationships between various paleointensity selection statistics and the inaccuracy of results

	Control (n = 160)		Historical (n = 112)		Combined (n = 272)	
Statistic	MIC	P	MIC	P	MIC	P
$\lvert k' \rvert$	*0.614*	*<0.001*	*0.311*	*0.039*	*0.368*	*<0.001*
δCK	*0.378*[†]	*<0.001*[†]	0.209	>0.060	*0.251*[‡]	*0.012*[‡]
DRAT	*0.391*[†]	*<0.001*[†]	0.187	>0.060	*0.276*[‡]	*<0.001*[‡]
CDRAT	*0.320*[†]	*0.004*[†]	0.294	>0.060	*0.250*[‡]	0.014[‡]
DRATS	*0.331*[†]	*0.002*[†]	0.225	>0.060	*0.262*[‡]	*0.004*[‡]
Mean DRAT	0.214[†]	>0.060[†]	0.296	>0.060	0.208[‡]	>0.060[‡]
δpal	0.267[†]	>0.060[†]	0.242	>0.060	*0.269*[‡]	*0.002*[‡]
δTR	0.192	>0.060	0.228	>0.060	0.186	>0.060
DRAT$_{tail}$	0.267	>0.060	0.208	>0.060	0.181	>0.060
MD$_{vds}$	0.235	>0.060	0.224	>0.060	0.186	>0.060
δt*	0.275	>0.060	0.234	>0.060	0.198	>0.060

Selection statistic definitions are given in ref. 1. MIC varies between 0 and 1. P values ≤ 0.05 are considered significant and are italicized.

[†]n = 158.

[‡]n = 270.

1. Paterson GA, Tauxe L, Biggin AJ, Shaar R, Jonestrask LC (2014) On improving the selection of Thellier-type paleointensity data. *Geochem Geophys Geosyst* 15:1180–1192.

Other Supporting Information Files

Dataset S1 (XLSX)
Dataset S2 (XLSX)
Dataset S3 (XLSX)